

Structural characterization of nanocrystalline InN grown on porous silicon by reactive sputtering

L. S. CHUAH*, Z. HASSAN^a, S. S. NG^a, H. ABU HASSAN^a

Physics Section, School of Distance Education, Universiti Sains Malaysia, 11800 Minden, Penang, Malaysia

^aSchool of Physics, Universiti Sains Malaysia, 11800 Minden, Penang, Malaysia

In the present paper, we report results of indium nitride (InN) films grown at room temperature by reactive sputtering method on porous silicon (PS). The PS samples were prepared using photoelectrochemical (PEC) method on n-type silicon wafer with (111)-orientation. To fabricate porous structures, the samples were immersed into a mix-up of HF:Ethanol (1:1) with a current densities of 50 mA/cm² for 5 min, and subjected to external illumination from a 500 W ultraviolet (UV) lamp. The surface morphology and the crystalline structure of the InN films were characterized by scanning electron microscope (SEM) and X-ray diffraction (XRD). Structural analysis revealed nanocrystalline structure with crystallite size of 32 nm for these films. An extensive characterization of optical properties of InN layers were studied by Raman and Fourier transform infrared (FTIR) reflectance spectroscopy at room temperature (300 K). Raman result showed that A₁(LO) (longitudinal optical phonons) of hexagonal InN has been observed at 588.4 cm⁻¹. From the result of FTIR spectroscopy, the TO [E₁(TO)] phonon mode of the InN is clearly visible at 472 cm⁻¹.

(Received September 15, 2008; accepted January 26, 2011)

Keywords: InN, Reactive sputtering, SEM, XRD, Raman, Porous silicon

1. Introduction

Among group III-nitrides, indium nitride (InN) is receiving increased attention because it enlarges the range of applications of nitrides to the visible and infrared (IR) spectral region. It is found to have good electron transport and optical properties. Moreover, InN has the smallest effective mass (0.12 m_e) leading to high mobility in pure material which makes it possible in the applications of high speed electronic devices. InN has a direct intrinsic bandgap, ranging from about 0.7 eV to 1.9 eV [1]. The discrepancy in bandgap could be attributed to the crystallinity, defects and impurities present in the material. InN also has various applications in optoelectronic devices such as light emitting diodes in the visible region, low cost solar cells with high efficiency, laser diodes (LDs), optical coatings, and optical waveguides [2]. Lately, it has acquired further concentration for the properties of its alloys with GaN and AlN which consent the fabrication of InGaAlN based short wavelength semiconductor laser diodes [3-5].

The fundamental problems in producing InN thin films are low dissociation temperature of InN and relatively low melting point of indium metal [1-2]. Various methods have been used to fabricate InN films, such as molecular beam epitaxy (MBE), metalorganic chemical vapor deposition (MOCVD), and pulsed laser deposition (PLD). However, reactive sputtering has been the most ordinarily applied as well as a approximately low priced technology for growth of polycrystalline InN films [6-7]. Situated on electrical transport properties, the high quality InN films have been coated by reactive sputtering [8]. It is renowned that the repress of reactive gases is particularly important for the optimization of films in reactive sputtering methods and it is not essential to

execute the sputtering in pure nitrogen for acquiring nitride films.

Sapphire substrate is commonly used for InN growth, although the difference between InN and sapphire is as large as 25 %. In this work, Si(111) substrate is used as an alternative substrate because of the attractive advantages, such as low-cost, availability of large size wafers, and mature processing techniques. The lattice mismatch between InN and Si is 8 % [9]. From the literature, growth of InN films on porous samples has not much studied. In recently, porous semiconductors have been popularly studied, fundamentally because of the dormant for purposeful engineering of properties not promptly gained in the corresponding crystalline precursors as well as the potential applications in optoelectronics, chemical and biochemical sensing [10-11]. When porosity is developed, these materials show different peculiar optical appearance, as an example, the displacement of bandgap, luminescence intensity improvement, and photoresponse enrichment [11-15]. Furthermore, porous semiconductor are under investigate as conceivable templates for epitaxial growth where the pores might perform as sinks for mismatch dislocations and furnish elastic strain in heterostructures [11, 16]. We present a report results of indium nitride (InN) films grown at room temperature by reactive sputtering method on porous silicon (PS).

2. Experimental details

Previous to the RF sputter deposition, the porous samples were adapted applying photoelectrochemical (PEC) technique. The silicon wafers used in this work were n-type phosphorus silicon wafer with (111)-orientation. The Si(111) samples were etched into a mixture of HF:Ethanol (1:1) for 5 minutes with a current

densities of 50 mA/cm^2 , and subjected to external illumination with a 500 W UV lamp and afterward well cleaned in de-ionized water. Fig. 1 presented the typical PEC wet etching equipment. The anodization is executed in potentiostatic (voltage-controlled) style. Structural properties of porous silicon (PS) have been investigated by scanning electron microscope (SEM) and X-ray diffraction (XRD).

InN films were fabricated by magnetron reactive sputtering deposition technology from indium targets (purity 99.999 %) in a mix-up gas of argon (Ar) and nitrogen (N_2). The substrate was kept at room temperature during the deposition. The sputtering system consists of a vacuum chamber with target and a turbo molecular pump parallel to a rotary pump to provide high vacuum circumstance, a RF power supply at 13.56 MHz, and mass flow controllers to maintain steady gas flow rate. The target was cleaned with a 5 min pre-sputter by Ar plasma prior to each deposition process. The growth conditions for InN films are summarized in Table 1.

Following the deposition, the thickness of InN film was studied by a surface step profile analyzer. The surface morphology of the samples was examined using SEM (JOEL JSM-6460LV). The crystalline structure of the InN films was characterized by X-ray diffraction (XRD).

The optical properties of InN layers were investigated by Raman spectroscopy at room temperature. Micro-Raman scattering experiments were performed by using a Jobin Yvon HR 800 UV spectrometer system. The excitation light source was the 514.5 nm line of Ar ion laser and the incident laser power was 20 mW.

Room temperature IR measurements are performed out by applying a Fourier transform infrared (FTIR) spectrometer with a KBr beam splitter and a middle infrared triglycine sulfate detector. The number of scans is 128. The measurements are captured in the reflection form at a resolution of 4 cm^{-1} and. A Perkin-Elmer changeable acute angle reflectance assistant is applied to count the reflectance spectrum at an incident angle of 15° [17].

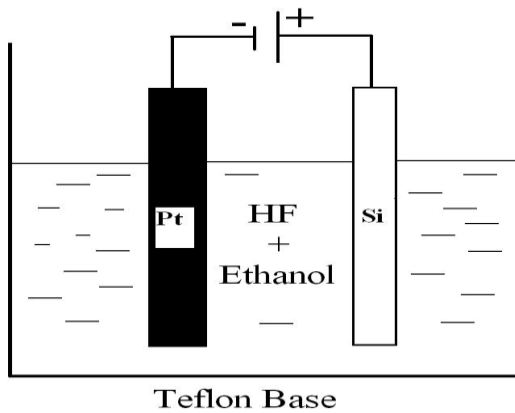


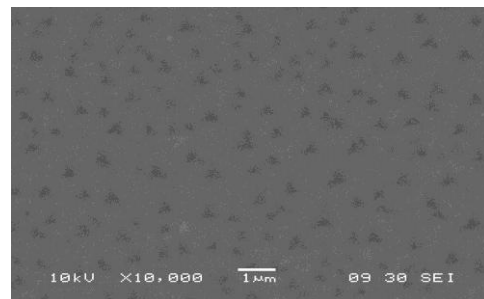
Fig. 1. Schematic diagrams of photoelectrochemical (PEC) wet etching apparatus [18].

Table 1. The deposition condition for InN film [18].

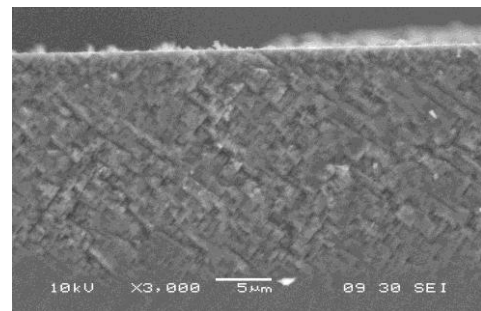
Target	Indium (99.999 %)
Target diameter	Three inch
Target-substrates distances	$\sim 15 \text{ cm}$
Substrate	Porous silicon (111)
Residual pressure	$< 4 \times 10^{-6} \text{ Torr}$
RF power	60 -70 W
Gas	$\text{N}_2 + \text{Ar}$ mixture
Gas ratio ($\text{N}_2:\text{Ar}$)	75 % : 25 %
Sputtering ambient	N_2 (99.995 %)
Gas flow rate (N_2 : Ar)	30 : 10 sccm
Sputtering pressure	$2.0 \times 10^{-2} \text{ Torr}$
Substrate temperature	Room temperature ($\sim 25^\circ \text{C}$)
Deposition time	90 min

3. Results and discussion

Fig. 2 shows the plan view and cross sectional view of porous silicon prepared on n-type Si(111). The thickness of the PS cross section is about $13 \mu\text{m}$. As presented in these figures, the silicon layer shows triangular-like uniform microarray which appears to be denser on the surface. Triangular microvoids formed by the rigid triangular shaped microarray network of 300 – 400 nm sizes is clearly seen in the plan view SEM image. The characteristic faceted, triangular shaped pores illustrate an orientation dependence of the photo anodization process of the Si(111) material.



(a)



(b)

Fig. 2. SEM images of porous silicon layers on n-Si (111) by PEC - etching (a) plan - view specimen (b) cross-sectional specimen.

Fig. 3 shows the XRD phase analysis scan of porous and as grown silicon. The intensity data was compiled by performing ω (sample angle) - 2θ (detector angle) scan at a limit of different values. The peaks at about 28.48° and 58.92° correspond to (111) and (222) diffraction peaks of silicon. It was found that the porous samples showed broader full width at half maximum (FWHM) than the single crystal sample for (111) diffraction planes.

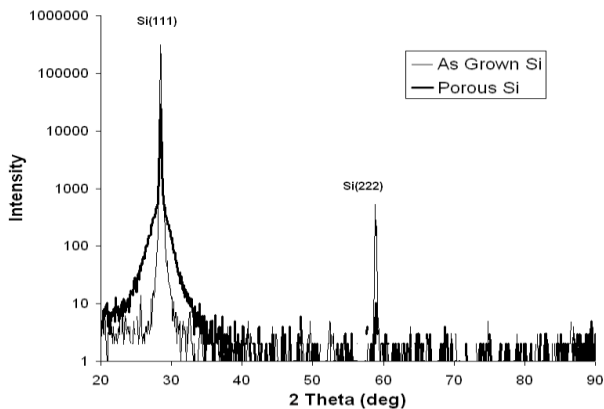


Fig. 3. XRD phase analysis scans of porous silicon and as grown silicon.

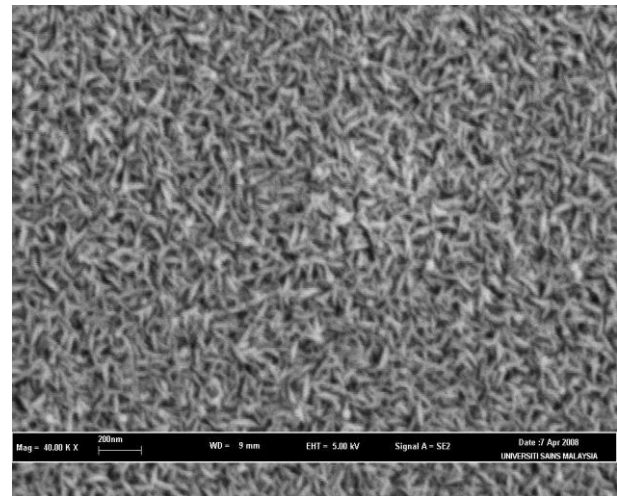
The surface morphologies and cross sectional view of InN film grown on porous silicon (PS) investigated using SEM are presented in Fig. 4. The thickness of the InN cross section from the SEM image is about 201 nm which is in good agreement with the thickness of InN film determined by a surface step profile analyzer which is about 200 nm. The deposited films were transparent and dark brown. It can be seen that the film consists of agglomerated nanocrystals. The pattern of the particles is a outcome of lattice mismatched materials where the nucleation of the nitride film is initiated on protruding crystals on the rough underlying substrate [18].

Fig. 5 shows a typical X-ray diffraction of the InN film grown on the porous silicon substrate. Only the peak from (101) InN plane is observed apart from the (111) peak from the porous silicon substrate. The c -axis orientation was not observed in our sample. The low intensity of the InN peak and a broadening centered at the crystalline region could be an indication that these films are a mixed phase of crystalline and amorphous structure [18]. This is seemingly a mark of the nanocrystalline phase for InN. The average size of the crystallites was determined from the (101) peak using the Scherrer formula [19]:

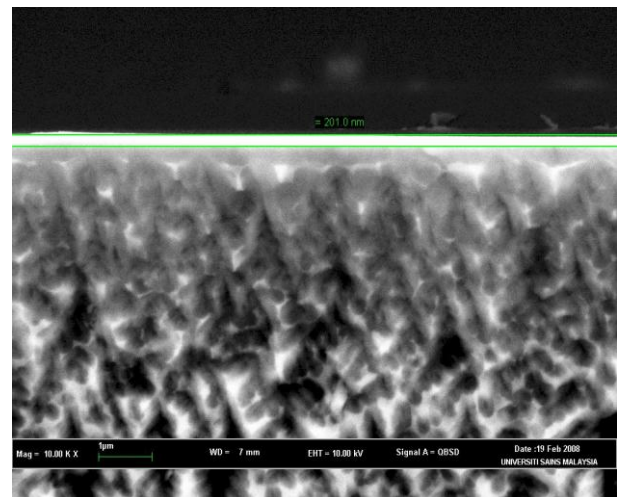
$$t = K\lambda / \beta \cos\theta \quad (1)$$

where t is the crystallite size, K is a constant, which is 0.9, λ is the wavelength of the incident beam, β is the half width of the peak, and θ is the diffraction angle of the peak [20]. Using Eq. (1), the crystallite (grain) size resolved by

the Scherrer method is nearly 32 nm, therefore confirming the nanocrystalline structure of our films.



(a)



(b)

Fig. 4. SEM images of InN film grown on porous silicon substrate (a) plan-view specimen (b) cross-sectional specimen.

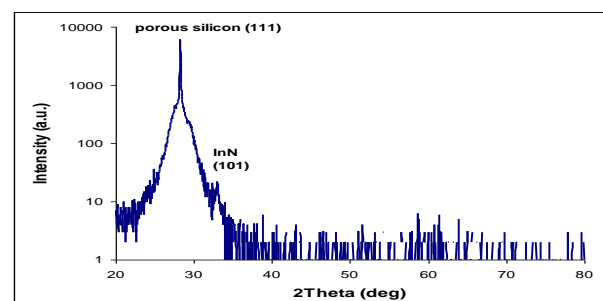


Fig. 5. XRD phase analysis scan of InN film grown on porous silicon.

The micro-Raman scattering experiments were carried out in the $z(x, \text{unpolarized})\bar{z}$ scattering configuration,

with z parallel to the c axis. Under this configuration, the allowed zone-center phonon modes that can be detected for wurtzite structure layer will be $A_1(\text{LO})$, $E_2(\text{Low})$, and $E_2(\text{High})$, unless there are some disoriented microstructures. The A_1 modes give atomic displacements along the c -axis, while the others, the E_2 give atomic displacements perpendicular to the c -axis [18].

Fig. 6 shows the room temperature Raman spectrum of InN thin films grown on porous Si substrate as well as the Raman spectrum of porous Si substrate [18]. The peak at 300.2 cm^{-1} comes from the Raman scattering of Si substrates. For InN thin film, only the allowed Raman phonon mode of $A_1(\text{LO})$ is clearly visible at 588.4 cm^{-1} [18]. In comparison to the result gained from the Davydov et al. [16], it is detected that the $A_1(\text{LO})$ mode of wurtzite InN is changed (about 2 cm^{-1}) moving to higher frequency. This difference can be ascribed to the quality of the InN thin film as well as the coupling effects between the LO and the free carrier concentrations, for example, noted as the LO plasmon-phonon (LPP) coupling properties [18]. The InN Raman mode of $E_2(\text{High})$, which is located at 488 cm^{-1} , is hardly detected from the spectrum because it has been masked by the stronger Si peak (at 520 cm^{-1}). The Raman mode of $E_2(\text{Low})$, located at 87 cm^{-1} [21], is invisible from the spectrum because of the cut-off limit of the 514.55 nm notch filter used in this work.

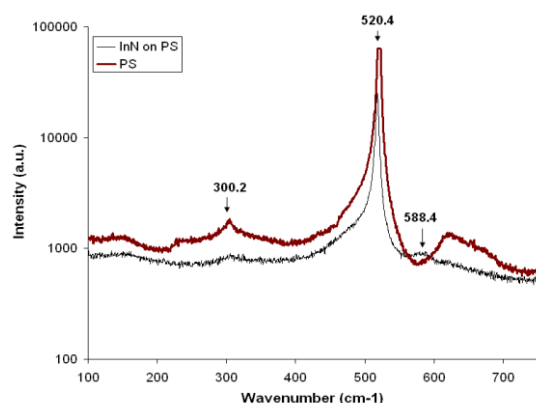


Fig. 6. Room temperature micro-Raman spectra of InN/porous silicon and porous silicon [18].

Fig. 7 shows the IR reflectance spectrum of InN thin films grown on porous Si substrate. For comparison, the IR reflectance spectrum of porous Si substrate is presented. In comprehensive, the InN reststrahlen area lies among 400 and 600 cm^{-1} while on the contrary the Si is inactive in infrared part. For InN thin film, the feature corresponds to the TO [$E_1(\text{TO})$] phonon mode of the InN is clearly seen at 472 cm^{-1} , which is comparable to the reported value for wurtzite InN [22]. Nevertheless, the prominent part (dip) due to the LO [$A_1(\text{LO})$] phonon mode of the InN (positioned at around $580 - 590\text{ cm}^{-1}$) was not perceived. This is principally due to the robust characteristics of its spectral strength as compared to the $E_1(\text{TO})$ form. For porous Si, the fringes are nearly all obviously because of interference among the radiations reflected from the top surface of the Si and that reflected from the pores [18].

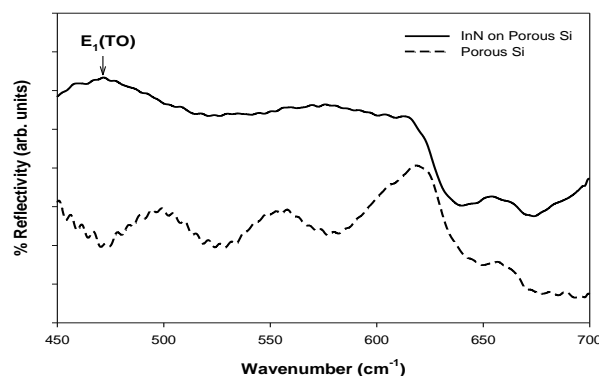


Fig. 7. IR reflectance spectrum of InN thin films grown on porous Si substrate.

4. Conclusion

Indium nitride (InN) films has been grown at room temperature by reactive sputtering method on porous silicon (PS). SEM, XRD, FTIR and Raman scattering were used to characterize the InN thin films. For porous silicon, triangular microvoids formed by the rigid triangular shaped microarray network of $300 - 400\text{ }\mu\text{m}$ sizes is clearly seen in the plan view SEM image. The nanocrystallite (grain) size of the InN film calculated by the Scherrer method is approximately 32 nm . For InN thin film, only the allowed Raman phonon mode of $A_1(\text{LO})$ is distinctly observed at 588.4 cm^{-1} . From the IR reflectance spectrum of InN, the feature corresponding to the TO [$E_1(\text{TO})$] phonon mode of the InN is precisely seen at 472 cm^{-1} , which is comparable to the reported value for wurtzite InN.

Acknowledgements

This work was supported by FRGS Grant. Financial support from Universiti Sains Malaysia is gratefully acknowledged.

References

- [1] F. K. Yam, Z. Hassan, Superlattices and Microstructures, **43**, 1 (2008).
- [2] S. J. Patil, Dhananjay S. Bodas, A. B. Mandale, S. A. Gangal, Thin Solid Film. **444**, 52 (2003).
- [3] I. Akasaki, S. Sota, H. Sakai, T. Tanaka, M. Koike, H. Amano. Electron. Lett. **32**, 1105 (1996).
- [4] S. Nakamura, M. Senoh, S. Nagahama, N. Iwasa, T. Yamada, T. Matsushita, H. Kiyoku, Y. Sugimoto, Jpn. J. Appl. Phys. **35**, L74 (1996).
- [5] Q. X. Guo, A. Okada, M. Nishio, H. Ogawa, Applied Surface Science, **169-170**, 345 (2001).
- [6] Z. G. Qian, G. Yu, W. Z. Shen, H. Ogawa, Q. X. Guo, Physica B, **318**, 180 (2002).
- [7] N. Saito, Y. Igasaki, Applied Surface Science, **169-170**, 349 (2001).

- [8] T. L. Tansley, C. P. Foley, *J. Appl. Phys.* **59**, 3241 (1986).
- [9] X. H. Ji, S. P. Lau, H. Y. Yang, Q. Y. Zhang, *Thin Solid Films*, **515**, 4619 (2007).
- [10] Xiuling Li, Young-Woon Kim, Paul W. Bohn, Ilesanmi Adesida, *Appl. Phys. Lett.* **80**, 980 (2002).
- [11] F. K. Yam, Z. Hassan, L. S. Chuah, Y. P. Ali, *Applied Surface Science*, **253**, 7429 (2007).
- [12] H. Hartono, C. B. Soh, S. Y. Chow, S. J. Chuah, E. A. Fitzgerald, *Appl. Phys. Lett.*, **90**, 171917 (2007).
- [13] M. A. Steven-Kaleeff, I. M. Tiginyanu, S. Langa, H. Foll, H. L. Hartnagel, *J. Appl. Phys.* **89**, 2560 (2001).
- [14] U. Rossow, *Phys. Status Solidi A*, **184**, 51 (2001).
- [15] A. El-Bahar, S. Stolyarova, A. Chack, R. Weil, R. Beserman, Y. Nemirovsky, *Phys. Status Solidi (A)*, **197**, 340 (2003).
- [16] D. J. Diaz, T. L. Williamson, L. Adesida, P. W. Bohn, R. J. Molnar, *J. Appl. Phys.* **94**, 7526, 1628833 (2003).
- [17] S. S. Ng, Z. Hassan, H. Abu Hassan, *J. Vac. Technol., A* **25**, 1557 (2007).
- [18] L. S. Chuah, Z. Hassan, S. S. Ng, H. Abu Hassan, *Journal of Alloys and Compound*, **479**, L54 (2009).
- [19] D. Y. Lee, I. S. Kim, J. S. Song, *Jpn. J. Appl., Phys.* **41**, 4659 (2002).
- [20] P. Scherrer, Estimation of the size and internal structure of colloidal particles, *Nachr. Ges. Wiss. Gottingen*; 1918. P. 96-100.
- [21] V. Y. Davydov, V. V. Emtsev, I. N. Goncharuk, A. N. Smirnov, V. D. Petrikov, V. V. Mamutin, V. A. Vekshin, S. V. Ivanov, M. B. Smirnov, T. Inushima, 1999 *Appl. Phys. Lett.*, **75**, 3297 (1999).
- [22] A. H. Bhuiyan, A. Hashimoto, A. Yamamoto, *J. Appl. Phys.*, **94**, 2779 (2003).

*Corresponding author: chuahleesiang@yahoo.com,
zai@usm.my